Acta Crystallographica Section D
**Biological Crystallography**
ISSN 0907-4449

# Novel c-di-GMP recognition modes of the mouse innate immune adaptor protein STING

**Ko-Hsin Chin,[a]‡ Zhi-Le Tu,[b]‡ Yi-Che Su,[b]‡ Yu-Jen Yu,[b] Hui-Chen Chen,[c] Yuan-Chao Lo,[d] Chin-Pan Chen,[d] Glen N. Barber,[e] Mary Lay-Cheng Chuah,[f] Zhao-Xun Liang[f] and Shan-Ho Chou[a,b,c]***

[a]Agricultural Biotechnology Center, National Chung Hsing University, Taichung 40227, Taiwan, [b]Institute of Biochemistry, National Chung Hsing University, Taichung 40227, Taiwan, [c]Graduate Institute of Basic Medical Science, China Medical University, Taichung 40402, Taiwan, [d]Institute of Biomedical Sciences, Academia Sinica, Taipei 115, Taiwan, [e]Department of Cell Biology, University of Miami School of Medicine, Miami, Florida, USA, and [f]School of Biological Sciences, Nanyang Technological University, Singapore 637551, Singapore

‡ K-HC, Z-LT and Y-CS made equal contributions to this manuscript and can be considered co-first authors.

Correspondence e-mail: shchou@nchu.edu.tw

Received 12 September 2012
Accepted 16 November 2012

**PDB References:** mSTING-CTD, 4g3l; mSTING-CTD–c-di-GMP complex, 4g4d

The mammalian ER protein STING (stimulator of interferon genes; also known as MITA, ERIS, MPYS or TMEM173) is an adaptor protein that links the detection of cytosolic dsDNA to the activation of TANK-binding kinase 1 (TBK1) and its downstream transcription factor interferon regulatory factor 3 (IFN3). Recently, STING itself has been found to be the direct receptor of bacterial c-di-GMP, and crystal structures of several human STING C-terminal domain (STING-CTD) dimers in the apo form or in complex with c-di-GMP have been published. Here, a novel set of structures of mouse STING-CTD (mSTING$^{137–344}$) in apo and complex forms determined from crystals obtained under different crystallization conditions are reported. These novel closed-form structures exhibited considerable differences from previously reported open-form human STING-CTD structures. The novel mSTING structures feature extensive interactions between the two monomers, a unique asymmetric c-di-GMP molecule with one guanine base in an unusual *syn* conformation that is well accommodated in the dimeric interface with many direct specific interactions and two unexpected equivalent secondary peripheral c-di-GMP binding sites. Replacement of the amino acids crucial for specific c-di-GMP binding in mSTING significantly changes the ITC titration profiles and reduces the IFN-$\beta$ reporter luciferase activity. Taken together, these results reveal a more stable c-di-GMP binding mode of STING proteins that could serve as a template for rational drug design to stimulate interferon production by mammalian cells.

## 1. Introduction

The innate immune system serves as a crucial sensor for monitoring the presence of foreign DNA or RNA in the extracellular space or cytosolic compartments (Hornung & Latz, 2010; Barbalat *et al.*, 2011; Barber, 2011). Toll-like receptors (TLRs) are important components for recognizing extracellular or endosomal nucleic acids and have been extensively studied in the past decade (Kawai & Akira, 2010; Barbalat *et al.*, 2011). More recently, nucleic acid sensors in the cytosol have emerged as a front line in the arsenal of the host's defence systems (Rathinam & Fitzgerald, 2011) and numerous unique receptors that guard the cytosolic compartments have been unveiled over the past several years (Barbalat *et al.*, 2011; Rathinam & Fitzgerald, 2011). Identification of foreign nucleic acid molecules *via* these cytosolic sensors can lead to the production of type I IFNs (Hornung & Latz, 2010; Takeuchi & Akira, 2010) to eliminate the invaders. The mammalian stimulator of interferon genes (STING; Ishikawa & Barber, 2008), also known as MITA (Zhong *et al.*, 2008), ERIS (Sun *et al.*, 2009), MPYS (Jin *et al.*, 2011) or TMEM173, is one of these

sensors and is predominately present in the endoplasmic reticulum (ER) membrane. It has been found to play a crucial role in linking the detection of cytoplasmic DNA to the phosphorylation of interferon regulatory factor 3 (IRF3) by TANK-binding kinase 1 (TBK1; Tanaka & Chen, 2012). The phosphorylated IRF3 then dimerizes and translocates into the nucleus to bind at the IFN-$\beta$ promoter to generate interferon and the expression of IL-1 family cytokines (Barber, 2011).

Cyclic di-GMP (c-di-GMP) is a unique secondary messenger that controls a plethora of bacterial activities including biofilm formation, biogenesis of flagella and pili, secretion of pathogenic factors *etc.* (Römling *et al.*, 2005; Hengge, 2009; Schirmer & Jenal, 2009). It interacts with a wide variety of protein-based or RNA-based recognition motifs. Some representative examples include the transcriptional factor Clp (Leduc & Roberts, 2009; Chin *et al.*, 2010; Tao *et al.*, 2010), degenerate GGDEF or EAL domains (Navarro *et al.*, 2009), PilZ-domain proteins (Amikam & Galperin, 2006; Benach *et al.*, 2007; Chin *et al.*, 2012) and riboswitches (Kulshina *et al.*, 2009; Smith *et al.*, 2009). However, the search for novel c-di-GMP effectors and their functions is still ongoing (Römling, 2012; Sondermann *et al.*, 2011; Krasteva *et al.*, 2012; Ryan *et al.*, 2012). Intriguingly, c-di-GMP has recently been found to be a potent activator of type I interferon response in mammalian hosts (Karaolis *et al.*, 2007; McWhirter *et al.*, 2009; Jin *et al.*, 2011; Sauer *et al.*, 2011). Furthermore, the C-terminal domain of STING (STING-CTD) has been identified to be the direct c-di-GMP binder (Burdette *et al.*, 2011). Structural studies are required to better characterize the interactions between STING and c-di-GMP or other cognate binding proteins.

During the preparation of this manuscript, five reports of crystal structures of human STING-CTD (human STING-CTD and mouse STING-CTD are abbreviated as hSTING and mSTING, respectively, in the following) in apo and c-di-GMP-bound forms have been published which appear to define a similar set of open-form structures (Huang *et al.*, 2012; Ouyang *et al.*, 2012; Shang *et al.*, 2012; Shu *et al.*, 2012; Yin *et al.*, 2012). In these structures, the originally predicted transmembrane helix comprising residues 153–173 is found to be present in the cytosol and participates in forming an active STING dimer. The binding of c-di-GMP does not notably change the hSTING conformation, but stabilizes the hSTING dimer to enhance its interaction with TBK1. However, the c-di-GMP in these structures makes few residue-specific interactions with the hSTING dimer; most binding residues seem to interact with c-di-GMP indirectly *via* mediating water molecules. These observations seem to indicate that another binding mode exists.

In this report, we describe a novel set of mSTING crystal structures in apo and c-di-GMP-bound forms that were determined from crystals obtained under different screening conditions and crystallized in different space groups. The newly determined mSTING apo and c-di-GMP-bound structures are more closed and compact, with c-di-GMP deeply buried inside the cleft formed by the subunit interface with marked asymmetry and one guanine base in an unusual *syn* conformation. In addition, two peripheral secondary c-di-GMP binding sites comprising a highly conserved and charged loop were revealed by the crystal structure and validated by solution binding measurements and *in vivo* cell assay data.

## 2. Materials and methods

### 2.1. Reagent and sample preparation for crystallography

c-di-GMP was produced by an enzymatic method using an altered thermophilic DGC enzyme as described previously (Rao *et al.*, 2009).

The sample preparation for truncated mSTING$^{138–344}$ and its complexes with c-di-GMP have been reported in a previous communication (Su *et al.*, 2012). In brief, the full-length *Mus musculus* (mouse) STING gene was synthesized using a two-step PCR-based DNA-synthesis method using *Escherichia coli* optimized codons (Xiong *et al.*, 2008). A series of mSTING gene fragments of different lengths were amplified by the PCR method with cognate primers. The obtained PCR fragments were cloned into the pET28 vector and were overexpressed in *E. coli* BL21 (DE3). Different SeMet-labelled mSTING truncations were prepared in a similar way using the non-auxotrophic *E. coli* strain Rosetta (DE3). Surprisingly, exclusion of the last putative transmembrane-containing region (residues 138–179; Burdette *et al.*, 2011) gave only inclusion bodies; only truncations starting from residue 138 delivered soluble proteins. However, only native and SeMet-labelled mSTING$^{138–344}$ truncations gave crystals that were suitable for further X-ray studies.

### 2.2. Construction of single-point mSTING mutants

All single-point mSTING mutants were generated using the QuikChange II site-directed mutagenesis kit (Stratagene; Vandeyar *et al.*, 1988) and the resulting sequences were further confirmed by DNA sequencing. All primers used in mSTING mutant generation are listed in Supplementary Table S1[1]. All mSTING variants were expressed and purified as described above.

### 2.3. IFN-$\beta$ promoter luciferase reporter assay

HEK293T cells were seeded on a 96-well plate for 24 h and were co-transfected transiently with 0.2 ng wild-type mSTING plasmid or the plasmid for the T262A or Q272A single mutants or the T262A/Q272A double mutant as well as with 20 ng IFN-$\beta$ promoter firefly luciferase reporter and 2 ng *Renilla* luciferase reporter (pRL-TK) plasmids. 24 h post-transfection, the HEK293T cells were stimulated with c-di-GMP using the digitonin permeabilization method as described previously (Woodward *et al.*, 2010) for 16 h. Firefly and *Renilla* luciferase activities were determined using the Dual Luciferase Assay System (Promega) and a Gloma 20/20 Luminometer (Promega) according to the manufacturer's

[1] Supplementary material has been deposited in the IUCr electronic archive (Reference: MN5017). Services for accessing this material are described at the back of the journal.

**Table 1**
Summary of the native and Se-SAD crystallographic data for mSTING and SeMet-mSTING.

Values in parentheses are for the outermost shell.

| | mSTING | SeMet-mSTING | mSTING–c-di-GMP |
|---|---|---|---|
| Beamline | BL13C1 | BL13B1 | SP44XU |
| Wavelength (Å) | 0.97622 | 0.97898 | 0.99808 |
| Space group | $P3_1$ | $P3_1$ | $P3_1$ |
| Unit-cell parameters (Å, °) | $a = b = 78.619$, $c = 50.418$, $\alpha = \beta = 90$, $\gamma = 120$ | $a = b = 78.493$, $c = 50.409$, $\alpha = \beta = 90$, $\gamma = 120$ | $a = b = 79.058$, $c = 49.693$, $\alpha = \beta = 90$, $\gamma = 120$ |
| Resolution range (Å) | 30–2.39 (2.48–2.39) | 30–2.20 (2.28–2.20) | 30–2.36 (2.44–2.36) |
| Total observations | 44542 (4387) | 125788 (12546) | 41778 (5210) |
| Unique observations | 13794 (1371) | 17676 (1767) | 14245 (1444) |
| Multiplicity | 3.2 (3.2) | 7.1 (7.1) | 2.9 (2.9) |
| Completeness (%) | 100 (100) | 100 (100) | 99.6 (100) |
| $R_{\rm merge}$† (%) | 6.1 (59.5) | 6.5 (44.7) | 3.9 (41.0) |
| $\langle I/\sigma(I)\rangle$ | 19.4 (2.3) | 23.8 (4.9) | 17.4 (2.8) |
| $R_{\rm free}$ test-set size (%) | 5 | 5 | 5 |
| Refinement statistics | | | |
| $R_{\rm cryst}$‡/$R_{\rm free}$§ (%) | 22.5/25.1 | 22.6/25.3 | 24.8/27.9 |
| Model content | | | |
| Protein residues | 370 | 370 | 378 |
| c-di-GMP molecules | 0 | 0 | 3 |
| $Mg^{2+}$ ions | 2 | 2 | 0 |
| Waters | 205 | 198 | 210 |
| Average $B$ factors (Å$^2$) | | | |
| Backbone atoms | 41.8 | 40.6 | 42.3 |
| Side-chain atoms | 43.6 | 42.8 | 45.9 |
| Water O atoms | 52.9 | 51.6 | 53.8 |
| c-di-GMP molecules | | | 59.2, 65.7, 68.3 |
| Ramachandran plot¶, residues in (%) | | | |
| Most favourable regions | 93.1 | 92.5 | 90.5 |
| Additionally allowed regions | 6.9 | 7.5 | 9.5 |
| R.m.s.d. from ideal geometry | | | |
| Bonds (Å) | 0.008 | 0.008 | 0.019 |
| Angles (°) | 1.50 | 1.48 | 1.85 |

† $R_{\rm merge} = \sum_{hkl}\sum_i |I_i(hkl) - \langle I(hkl)\rangle|/\sum_{hkl}\sum_i I_i(hkl)$. ‡ $R_{\rm cryst} = \sum_{hkl}\big||F_{\rm obs}| - |F_{\rm calc}|\big|/\sum_{hkl}|F_{\rm obs}|$, where $F_{\rm calc}$ and $F_{\rm obs}$ are the calculated and observed structure-factor amplitudes, respectively. § $R_{\rm free}$ is the same as $R_{\rm cryst}$ but for 5.0% of the total reflections chosen at random and omitted from refinement. ¶ The percentages of residues located in the most favourable and additionally allowed regions were calculated using the *MolProbity* program with the default parameters (Chen *et al.*, 2010). No outliers were found.

protocol. The relative luciferase activity was expressed as firefly luminescence intensity relative to *Renilla* luminescence.

### 2.4. ITC experiments

The association constant ($K_a$) between mSTING and c-di-GMP was measured using an ITC200 calorimeter (MicroCal). Titrations of mSTING with c-di-GMP were carried out at 298 K in assay buffer consisting of 20 m*M* Tris–HCl pH 8.0, 80 m*M* NaCl, 1 m*M* $MgCl_2$. A sample of wild-type mSTING protein for ITC was dialyzed extensively against the assay buffer overnight. The concentration of mSTING in the cell was 0.2 m*M* and that of c-di-GMP in the syringe was 3 m*M*. For wild-type mSTING, 1 µl c-di-GMP was injected into the cell a total of 30 times, with a time lag of 150 s between each injection. ITC data were analyzed by integrating the amount of heat exchange after the background dilution heat had been subtracted from the apparent values. Data fitting was based on a single-site binding model; the commercial package provided (*Origin*) was used to obtain the values of $K_a$, $\Delta H$ and $\Delta S$. The $\Delta G$ value was derived using the equation $\Delta G = \Delta H - T\Delta S$.

### 2.5. Crystallization of truncated variants of mSTING

For crystallization, native and SeMet-labelled mSTING$^{138–344}$ were concentrated to approximately 6.5 mg ml$^{-1}$ in 20 m*M* Tris–HCl pH 8.0, 80 m*M* sodium chloride using an Amicon Ultra-10 (Millipore). Appropriate volumes of 0.5 m*M* c-di-GMP were also added to the solutions of native and SeMet-labelled mSTING$^{138–344}$ to prepare samples for mSTING–c-di-GMP co-crystallization at a ligand:protein monomer ratio of 2.0. Screening for crystallization conditions for SeMet-labelled and native mSTING$^{138–344}$ and their c-di-GMP-bound complexes were performed using sitting-drop vapour diffusion in 96-well plates (Hampton Research) at 277 K by mixing 0.5 µl protein solution with 0.5 µl reservoir solution and equilibrating against 50 µl reservoir solution. Pyramid-shaped crystals of mSTING$^{138–344}$ appeared in 7 d from drops equilibrated against 50 µl reservoir solution comprising 2% PEG 400, 1.6 *M* ammonium sulfate, 0.1 *M* MES monohydrate; pyramid-like crystals of SeMet-labelled mSTING$^{138–344}$ appeared in 7 d from drops equilibrated against 50 µl reservoir solution comprising 1.6 *M* potassium/sodium phosphate, 0.1 *M* Na HEPES pH 7.5 (Su *et al.*, 2012). Crystals of both proteins suitable for diffraction experiments were grown from drops obtained by mixing 1.5 µl protein solution with 1.5 µl reservoir solution and equilibrated against 500 µl reservoir solution at 277 K.

### 2.6. Data collection and processing

X-ray diffraction data for native mSTING and SeMet-labelled mSTING were collected on beamlines 13C1 and 13B1, respectively, at the National Synchrotron Radiation Research Center (NSRRC) in Taiwan and reached resolutions of 2.39 and 2.2 Å, respectively. The data for the mSTING–c-di-GMP complex were collected on the SP44XU beamline at the SPring-8 facility and reached a resolution of 2.36 Å. The data were indexed and integrated using the *HKL*-2000 processing software, generating data sets that were 100% complete in each case. All crystals of native mSTING and its c-di-GMP-bound complex were found to belong to space group $P3_1$. The heavy-atom search, phasing and density modification for SeMet-labelled mSTING were carried out using the *AutoSol* wizard (Terwilliger *et al.*, 2009) from the *PHENIX* suite (Adams *et al.*, 2010). A marginally good figure of merit (FOM) value of 0.308 was obtained from this Se-SAD

approach, leading to successful model building of the mSTING protein after running the *AutoBuild* program (Terwilliger *et al.*, 2008). The model was manually adjusted using the *XtalView*/*Xfit* package (McRee, 1999). *CNS* (Brünger *et al.*, 1998) was then used to refine the native mSTING structure to a final $R_{cryst}$ of 22.5% and $R_{free}$ of 25.1%. The mSTING structure was then used as the template for a molecular-replacement approach (Brünger *et al.*, 1998) to determine the phases of the mSTING–c-di-GMP complex, which was also successfully refined to a final $R_{cryst}$ of 24.8% and $R_{free}$ of 27.9%. Detailed data-collection and refinement statistics are summarized in Table 1.

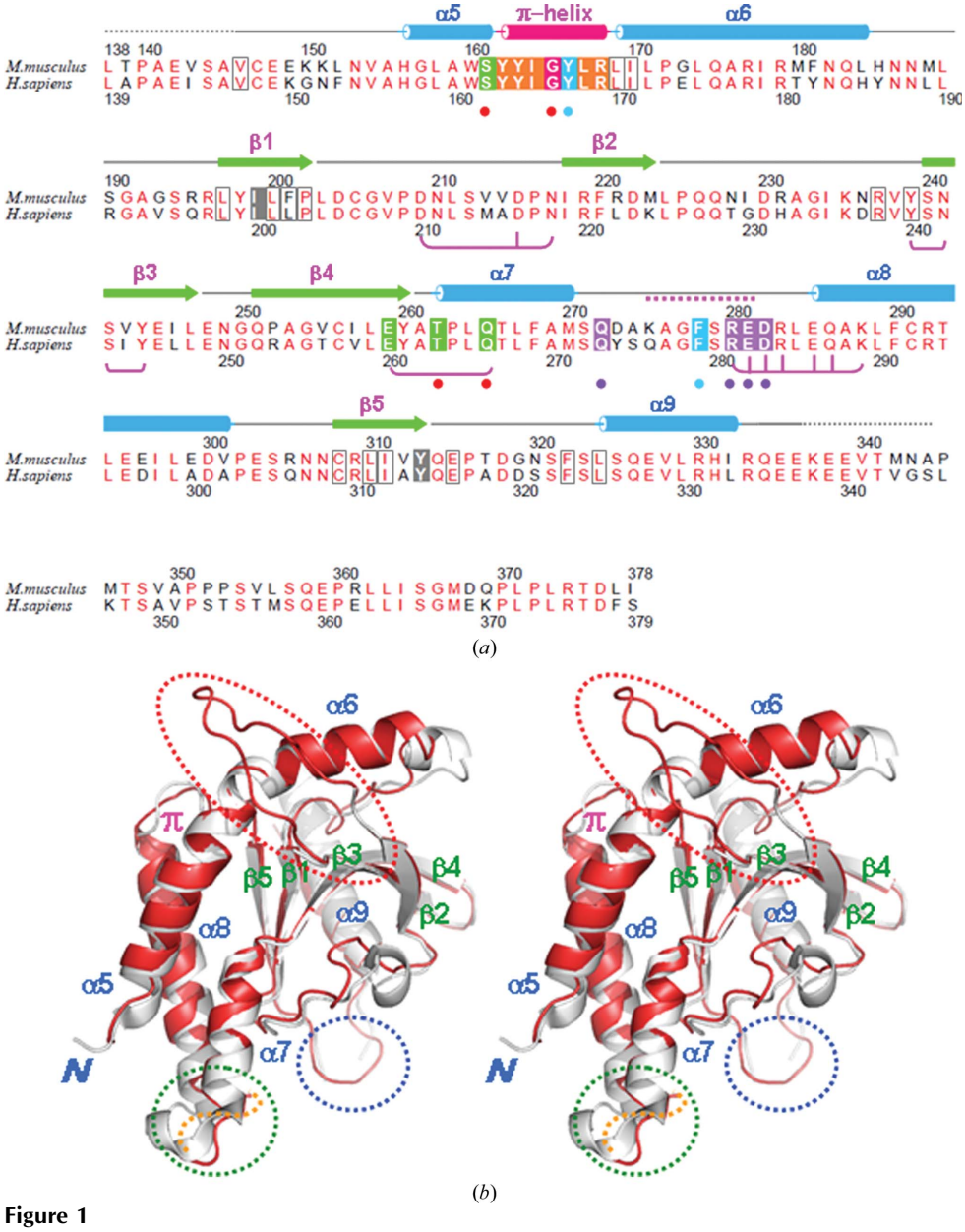


**Figure 1**
Sequence alignment and structural characterization of the mSTING and hSTING monomers. (*a*) Alignment of the C-terminal domain sequences of the mSTING and hSTING proteins. Invisible residues at the N-terminal and C-terminal ends are connected by dotted lines. Conserved residues are shown in red text. Secondary-structural elements (arrows, $\beta$-strands; tubes, $\alpha$-helices) are shown above the mSTING sequence. The $\pi$-helix between the $\alpha$5 and $\alpha$6 helices is coloured magenta with highlighted residues. Residues involved in interaction with interfacial c-di-GMP are marked by red dots, while those interacting with peripheral c-di-GMP are marked by purple dots, except for residues Tyr166 and Phe278, which form hydrophobic stacks with guanine bases and are marked by blue dots. Residues that were invisible before peripheral c-di-GMP binding are connected by a dotted red line above the sequence. Clustered altered residues that lead to a loss of c-di-GMP binding capability (Burdette *et al.*, 2011) are connected by horizontal brackets with altered residues marked by vertical lines. Two crucial residues, Ile199 and Tyr313, responsible for inducing IFN-$\beta$ production are involved in forming a stable hydrophobic core and are highlighted in grey. Some hydrophobic residues that interact with Ile199 or Tyr313 are boxed in grey. (*b*) Stereoview of the superimposition of the mSTING (shown as a red cartoon) and hSTING (shown as a grey cartoon) monomeric structures. The $\beta$2–$\beta$3 and $\beta$5–$\alpha$9 loops are invisible in hSTING and are circled by red and blue dotted lines, respectively, while the $\alpha$7–$\alpha$8 loop is invisible in mSTING and is circled by a green dotted line.

## 3. Results

### 3.1. Structural determination of mSTING

Fig. 1(*a*) shows a sequence alignment between the mouse and human STING C-terminal domains. The two sequences are rather similar, with no gaps (69% sequence identity). The native mSTING structure was determined to 2.2 Å resolution using a selenium single-wavelength anomalous dispersion (Se-SAD) approach. The quality of the electron-density map of the mSTING apo form is reasonably good from the N-terminal residue Val146 to the C-terminal residue Glu336, apart from the Lys275–Glu281 ($\alpha$7–$\alpha$8) loop, which comprises the secondary peripheral c-di-GMP binding site (described below) and is invisible before c-di-GMP binding (shown in magenta dots above the sequence in Fig. 1*a*). The solved monomeric mSTING structure is similar to those of hSTING published to date (Huang *et al.*, 2012; Ouyang *et al.*, 2012; Shang *et al.*, 2012; Shu *et al.*, 2012; Yin *et al.*, 2012). They superimpose rather well, with an r.m.s.d. of approximately 1 Å between the monomeric mSTING and hSTING (PDB entry 4ef5; Ouyang *et al.*, 2012) structures (Fig. 1*b*). Residues Asn153–Gly173 of mSTING do not form a transmembrane helix, but form a cytosolic helix that plays a critical role in forming

the dimeric interface and in binding to the c-di-GMP ligand (discussed below). However, one major difference between the mSTING structure and the reported hSTING structure (PDB entry 4ef5) is the clearly visible $\beta2$–$\beta3$ loop (marked in a dotted circle in red in Fig. 1*b*) and $\beta5$–$\alpha9$ loop (marked in a dotted circle in blue) in mSTING, which are invisible in the hSTING structure (Figs. 1*b* and 2*a*). These differences in loop visibility are likely to result in a more flexible and open nature of the hSTING apo-form structure compared with the more rigid and closed form of mSTING, which will be described in detail below.

### 3.2. The mSTING monomer contains a long N-terminal helix kinked twice by a $\pi$-helix and an internal proline

When interrupted by a proline residue, a long helix can be bent in the middle to increase the structural diversity of proteins. Recently, it has also been suggested that a $\pi$-helix, which has a wider diameter than a regular $\alpha$-helix, can also bend a helix (Weaver, 2000; Cooley *et al.*, 2010). A $\pi$-helix is characterized by an amino-acid insertion into a regular $\alpha$-helix without changing the helical pitch or rise. Hence, the helical diameter becomes wider and instead of the canonical $CO^{i}$–$HN^{(i+4)}$ intra-helical hydrogen bond usually observed in a regular $\alpha$-helix, two or more unique $CO^{i}$–$HN^{(i+5)}$ intra-helical hydrogen bonds are observed (Cooley *et al.*, 2010). In mSTING, we find that residues His156–Leu184 form a very long N-terminal helix that is interrupted in the middle by a $\pi$-helix (Fig. 1*a* and Supplementary Fig. S1). This long helix starts as the regular $\alpha5$ helix from residue His156 to residue Trp160, followed by a $\pi$-helix from residue Ser161 to residue Arg168. After this, the long helix returns to the regular $\alpha6$ helix, but is kinked again by an internal proline at position 172. Gly165 is the bulged-out amino acid in this $\pi$-helix, with a carbonyl group that points away from the intrahelical axis (marked by a dotted arrow in green in Supplementary Fig. S1*b*), and hence cannot form an intra-helical hydrogen bond with other amino acids in the helix. Two characteristic $CO^{i}$–$HN^{(i+5)}$ intra-helical hydrogen bonds between the adjacent residues Tyr162–Leu167 and Tyr163–Arg168 are observed (marked by dotted arrows in pink in Supplementary Fig. S1*b*). The long helix is thus kinked twice: once by approximately 15° by $\pi$-helix formation and again to a similar degree by the internal Pro172 (as revealed in Fig. 3*b*). Importantly, $\pi$-helix formation is usually found to be associated with protein function, and identification of such a characteristic structural element can help to identify a ligand-binding site in a protein. This is indeed the case in mSTING, since the central $\pi$-helix is found to participate in binding the c-di-GMP ligand to a great extent (Fig. 3).

### 3.3. Unliganded mSTING adopts a unique closed dimeric structure

Although the monomeric structure of mSTING is quite similar to the hSTING structures, dimeric mSTING adopts a closed and more compact structure, as revealed in Fig. 2(*a*); the hSTING dimer is found to form a wider V-shaped valley (grey cartoon and marked by blue dotted arrows in Fig. 2*a*) than the mSTING dimer (red cartoon and marked by orange dotted arrows in Fig. 2*a*). This is consistent with a larger dimeric interfacial contact area of 1188 Å$^2$ for mSTING compared with 939 Å$^2$ for hSTING (PDB entry 4ef5) as calculated using the *PISA* program (Krissinel & Henrick, 2007). The dimeric interfacial contact areas in mSTING mainly consist of two major segments: a top $\beta2$–$\beta3$ loop from residues Lys235 to Ser240 and residues Phe220 to Gln226 (Fig. 2*a* and Supplementary Fig. S2*a*) and a bottom $\alpha5$ helix from residues Leu152 to Leu158 (Fig. 2*b* and Supplementary Fig. S2*d*). The top region interacts through both hydrophobic interactions and hydrogen bonds (Supplementary Fig. S2*a*), while the bottom region interacts mainly through hydrophobic interactions (Supplementary Fig. S2*d*). The detailed interfacial

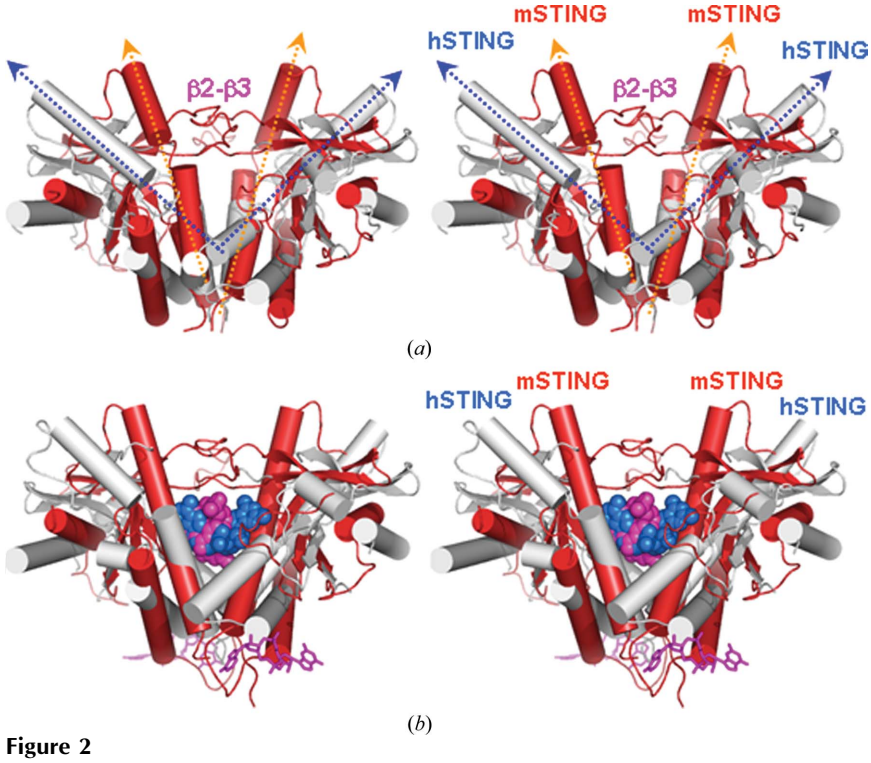


**Figure 2**
Superimposition of the mSTING and hSTING apo forms (*a*) and c-di-GMP-bound forms (*b*) in stereo. Cartoons of mSTING are coloured red, while those of hSTING are grey. Interfacial c-di-GMP in the mSTING complex is shown as spheres and coloured magenta, while that of hSTING is coloured blue. Peripheral c-di-GMP in the mSTING complex is drawn in stick representation and coloured magenta. A wider valley is observed for the hSTING structures (marked by dotted arrows in blue) than the mSTING structures (marked by dotted arrows in orange). The $\beta2$–$\beta3$ loop forms a lid to cover the ligand-binding sites in the mSTING apo-form and c-di-GMP-bound structures. However, this loop is invisible in the hSTING apo-form and c-di-GMP-bound structures.

polar interactions are listed in Supplementary Table S2. Such a closed unliganded form has less often been described in the literature (Floceo & Mowbray, 1994; Aparicio *et al.*, 2003; Bermejo *et al.*, 2010). The good interfacial interactions between the $\beta$2 and $\beta$3 strands may account for the preference of mSTING to form a more closed unliganded form.

It is worth noting that in its apo form mSTING already contains a ligand-binding pocket, which is enclosed by the two long $\beta$2–$\beta$3 loops at the top (Fig. 3*a*) and by the $\pi$-helix and $\alpha$7 helix at the two sides (Fig. 3*b*). Several water molecules are observed in the cavity and interact with the surrounding amino-acid residues (Figs. 3*b* and 3*c*). More water molecules may be present in the pocket, but are possibly more disordered and cannot be observed in the electron-density map. Importantly, these bound water molecules are released from the active site when c-di-GMP binds mSTING (Fig. 4*d*).

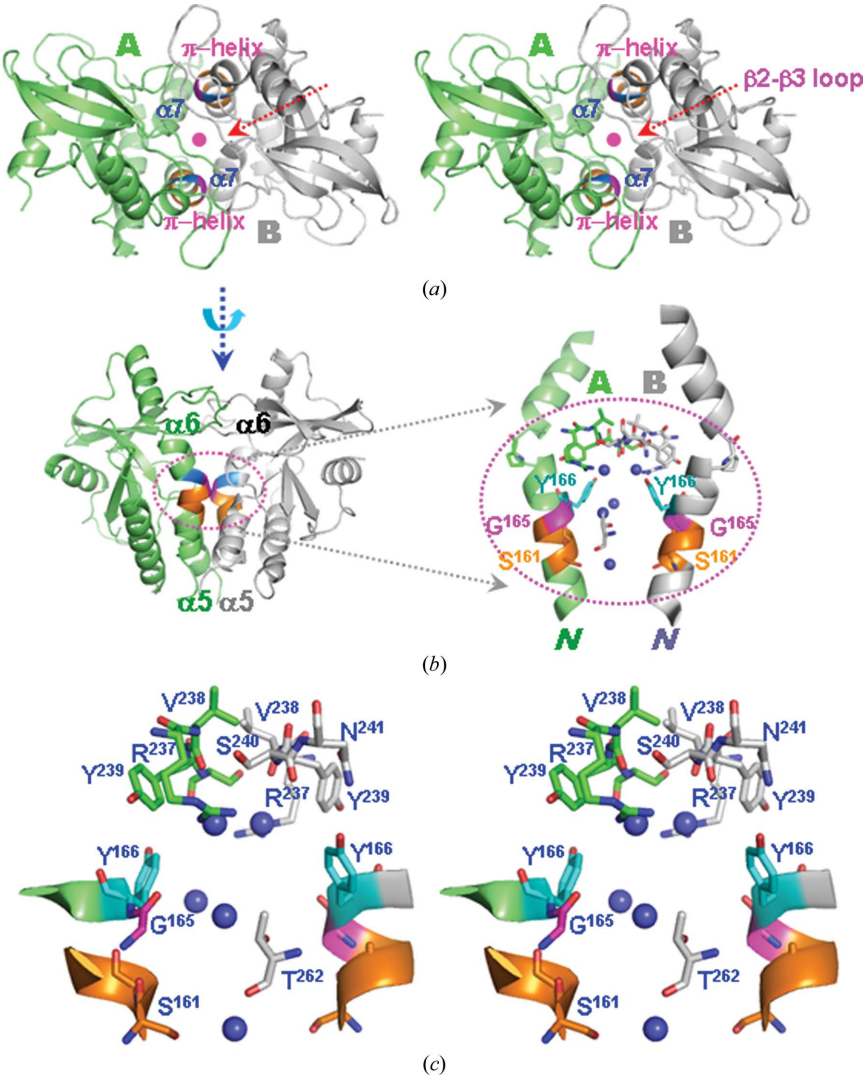


**Figure 3**
Structural features of the closed-form mSTING dimer. (*a*) Stereoview of the mSTING dimer viewed from the top. The twofold axis is indicated by a pink dot. The central ligand-binding pocket is enclosed by the $\beta$2–$\beta$3 loop at the top (indicated by a red dotted arrow) and by two $\pi$-helices (coloured red) and two $\alpha$7 helices at the sides. (*b*) Side view of the mSTING dimer (left). The twofold axis is shown at the top. The circled $\pi$-helix region is shown expanded on the right. The doubly kinked $\alpha$5–$\pi$–$\alpha$6 helix is clearly revealed in this figure. (*c*) Stereoview of the interfacial pocket of the mSTING dimer. Residues surrounding the ligand-binding site are marked. Five water molecules are observed and are shown as blue dots.

### 3.4. A unique binding mode of c-di-GMP in the mSTING–c-di-GMP complex

The mSTING–c-di-GMP complex was prepared by cocrystallizing c-di-GMP and mSTING at a ligand:protein molar ratio of 2.0. To determine their complex structure, we used the solved native mSTING structure as a template in a molecular-replacement approach. Since mSTING is very similar in its apo form and its complex form (Supplementary Fig. S4*a*), the molecular-replacement method was successfully applied to solve the structure of the mSTING complex (Fig. 4*a*). The model quality of the mSTING in the complex is quite good and can be traced from the initial residue Val146 to the C-terminal end residue Glu336, including the originally invisible loop residues responsible for binding the peripheral c-di-GMP comprising residues Lys276–Glu281 in the native mSTING structure (Fig. 1*b*). The interfacial contact area has therefore increased by approximately 10% from 1188 to 1351 Å$^2$. Detailed hydrogen-bond and electrostatic interactions for mSTING in the complex are listed in Supplementary Table S3. As expected, a large patch of electron density was found in the interfacial ligand-binding pocket (Fig. 4*b*). A c-di-GMP model was placed in the electron-density map, rearranged and refined to obtain a final c-di-GMP structure that can fit well into the electron-density map. The $F_o - F_c$ electron-density map of the interfacial c-di-GMP is observable for most atoms; it adopts a unique conformation that is very distinct from those observed in other reported complex structures (Fig. 4*b*).

All reported hSTING–c-di-GMP structures adopt a more open dimeric structure with only one ligand bound (one representative example, PDB entry 4ef4, is shown in Fig. 2*b* and Supplementary Fig. S3) and the bound c-di-GMP is found to interact with hSTING indirectly. For example, it interacts with hSTING primarily *via* $H_2O$-mediated hydrogen bonds; only the side-chain O atom of Thr264 is found to form two specific hydrogen bonds to the guanine N3 and O2′ atoms (Supplementary Fig. S3*b*; Ouyang *et al.*, 2012). Also, both guanine bases are found to face upwards and are exposed to solvent (Supplementary Fig. S3). In sharp contrast, mSTING adopts a unique closed-form dimeric structure with three c-di-GMP molecules observed in the crystal

structure (Fig. 4*a*). Some of the distinct features of the mSTING–ligand complex structure include (i) the c-di-GMP molecule tumbles 180° around the *x* axis, with both guanine bases facing downwards (Figs. 4*c* and 4*d*), (ii) c-di-GMP binds with marked asymmetry in the primary binding site owing to the flipping of the Gua2 base to form an unusual *syn* configuration (Fig. 4*d*) and (iii) c-di-GMP binds directly to the side-chain atoms of the surrounding active-site residues (Fig. 4*d*). These unique interactions are found to be promoted by the presence of the $\pi$-helix (Fig. 4*c*), with its Gua1 and Gua2 bases interacting well with Ser161, Gly165 and Tyr166 in the $\pi$-helix in an asymmetric way. For example, the Gua1 base forms a hydrogen bond (marked by a dotted blue arrow) to the side-chain O atom of Ser161 (Fig. 4*c*) and stacks with the backbone atoms of Gly165 (indicated by a thick dotted arrow in grey in Figs. 3*c* and 4*d*). Also, the Gua1 ribose atoms stack with the phenyl group of Tyr166 (Fig. 4*d*). However, it is the Gua2 base that interacts with Thr262 and stacks well with Tyr166 (Fig. 4*d*). Other than the interactions from the two sides, quite a few hydrogen bonds or electrostatic bonds from the top lid region are present to firmly accommodate the 12-membered macrolactone ring of c-di-GMP (Fig. 4*d*) in the interfacial ligand-binding site. Detailed interactions between mSTING and c-di-GMP in this binding site are listed in Supplementary Table S4. The mSTING–c-di-GMP complex thus adopts a unique closed liganded form, with its interfacial binding site well shielded from solvent. Interestingly, this closed liganded form does not exhibit a large conformational change from its closed unliganded form: they overlap well with an r.m.s.d. of only 0.86 Å over 346 $C^{\alpha}$ atoms (Supplementary Fig. S4*a*). However, considerable differences between the hSTING–c-di-GMP and mSTING–c-di-GMP complexes are observed

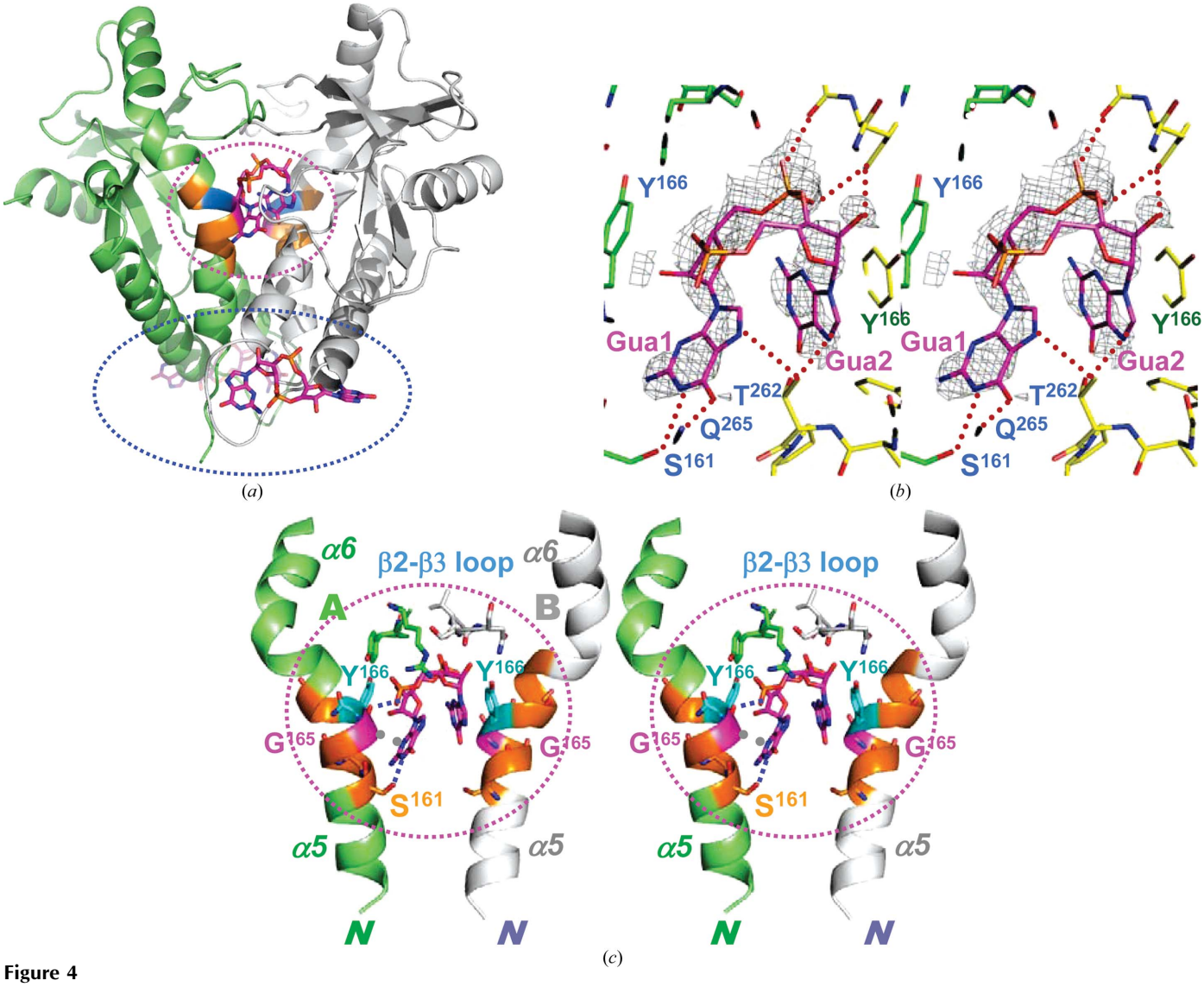


**Figure 4**
Structural features of the closed-form mSTING–c-di-GMP complex. (*a*) Crystal structure of the mSTING–c-di-GMP complex viewed from the side. One c-di-GMP molecule is bound in the interfacial region (circled by a dotted red line), while two c-di-GMP molecules are bound at the peripheral regions close to the $\alpha$7–$\alpha$8 helices (circled by a dotted blue line). (*b*) $F_o - F_c$ electron-density map of c-di-GMP in the mSTING active-site region drawn at the 1$\sigma$ contour level. C atoms of surrounding resides are shown in green and yellow for monomers *A* and *B*, respectively. (*c*) c-di-GMP is embedded in the $\pi$-helix (cartoon coloured in orange and blue) and topped by the $\beta$2–$\beta$3 loop.

(Fig. 2), which are reflected in their different binding-surface areas as measured using the *PISA* program. In the hSTING–c-di-GMP complex (PDB entry 4ef4) the surface contact area is 896 Å$^2$ between the hSTING subunits and 470 Å$^2$ between hSTING and ligand. Therefore, the contact area in the hSTING–c-di-GMP complex is 1366 Å$^2$ in total after ligand binding. However, in the mSTING–c-di-GMP complex the surface contact area is 1351 Å$^2$ between the mSTING subunits and 606 Å$^2$ between mSTING and ligand. A total surface contact area of 1957 Å$^2$ is observed after c-di-GMP binding.

### 3.5. The secondary peripheral c-di-GMP binding site in mSTING

Another interesting issue that was not observed in the previous structure of the hSTING–c-di-GMP complex is the discovery of a secondary peripheral c-di-GMP binding site at the $\alpha$7–$\alpha$8 loop region for each mSTING monomer (Fig. 4*a*). This peripheral binding site comprises residues Gln272–Asp282 linking the $\alpha$7 and $\alpha$8 helices (Fig. 1*a* and 5*b*). The $F_o - F_c$ electron-density map for c-di-GMP in the peripheral binding site is also observable, although not complete, possibly owing to its more dynamic nature since it is more exposed to solvent (Fig. 5*c*). Importantly, most of the surrounding residues (Ala274–Glu281) were originally unidentified in the apo form (Fig. 5*a*) but became visible after c-di-GMP binding (Fig. 5*b*), indicating that c-di-GMP binding stabilizes these loop residues. Unlike the c-di-GMP bound in the primary interfacial binding site, c-di-GMP in the peripheral binding site is more extended and exposed to the solvent (Fig. 5*b*), but still interacts with several residues in the $\alpha$7–$\alpha$8 loop region, including Gln272, Arg280, Glu281 and Asp282 (Fig. 4*b*). Intriguingly, these residues had been identified to bind c-di-GMP in a previous study and replacement of all these residues was found to abolish c-di-GMP binding capability, supporting the likely existence of the peripheral binding site (Burdette *et al.*, 2011; highlighted in purple in Fig. 1*a*).

To investigate whether mSTING binds more than one c-di-GMP molecule in solution, we have also conducted an extensive ITC study by titrating c-di-GMP against wild-type mSTING and numerous mSTING variants. We generated a total of 15 mSTING variants. Unfortunately, most of them formed inclusion bodies or were unstable and could not be used in ITC titration studies (Table 2). In the end, only five

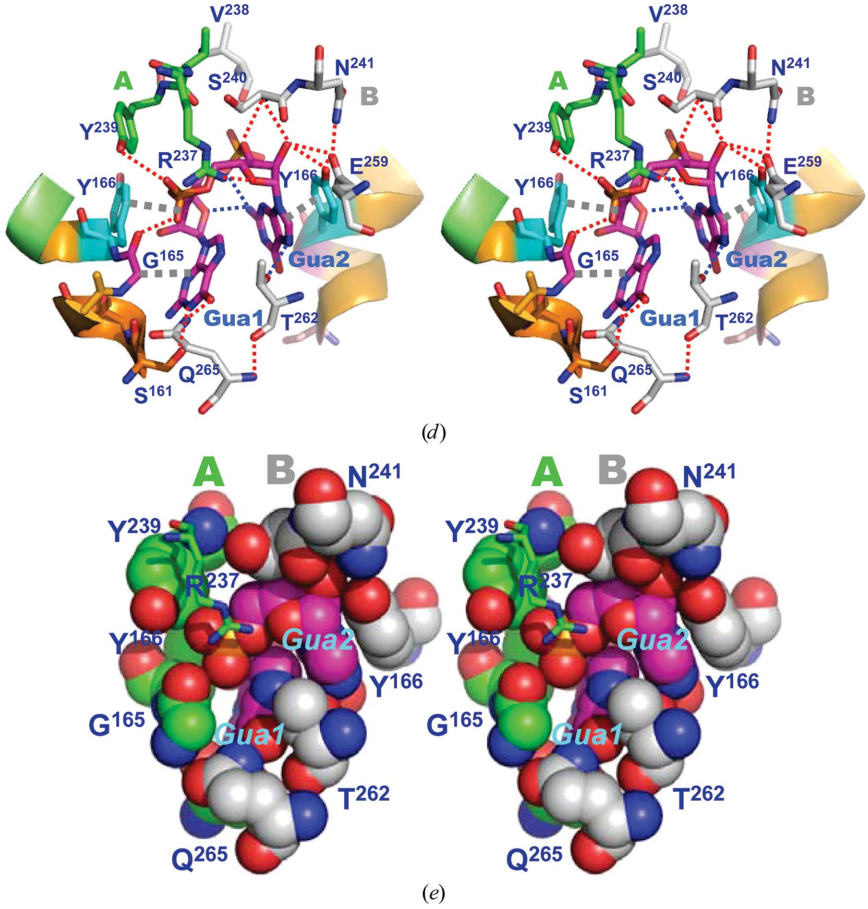


**Figure 4 (continued)**
(*d*) Close-up of the interfacial ligand-binding site showing detailed c-di-GMP–mSTING interactions. Hydrogen bonds or electrostatic bonds are shown as dotted lines in red, while hydrophobic stacking is shown as thick dotted lines in grey, except for the two intramolecular bonds of c-di-GMP, which are drawn as dotted lines in blue. C atoms of surrounding resides are shown in green and grey for subunits *A* and *B*, respectively, and those of c-di-GMP are in magenta. Gua1 adopts an antiglycosidic bond, while Gua2 adopts an unusual *syn*-glycosidic bond. (*e*) Similar region drawn in van der Waals spheres. Side-chain atoms of Thr262 interact extensively with c-di-GMP and are 'wedged' into its opening.

single-mutant variants, including three in the interfacial binding site (S161A, T262A and N241A) and two in the peripheral binding site (Q272A and D282A), could be employed to obtain stoichiometric values and other thermodynamic parameters (Table 2). To begin with, the titration experiment for wild-type mSTING was repeated many times and optimized by changing the concentrations of the mSTING protein and the c-di-GMP ligand, as well as the volume of c-di-GMP in each injection. Optimal results were obtained by injecting 1 µl 3 m*M* c-di-GMP into a sample cell containing 0.2 m*M* mSTING solution. From the optimized titration profile, we found that additional c-di-GMP binding sites are indeed present in the mSTING protein, as revealed by the peculiar biphasic profile (Fig. 5*d*). Cyclic nucleotide-binding proteins have a tendency to bind more than one ligand, as demonstrated by CRP (cAMP receptor protein), which can bind up to four cAMP molecules for the CRP dimer either in the crystal (Passner & Steitz, 1997) or in solution (Lin & Lee, 2002). Intriguingly, the wild-type mSTING titration data could be best fitted by a single-site model to obtain a ligand:protein monomer molar ratio of 1.5 or a ligand:protein dimer molar ratio of 3.0. This result indicates that in the wild-type mSTING three c-di-GMP binding sites (one interfacial and two peripheral) are present which have approximately similar binding constants ($K_d$ of $\sim 10^{-7}$). However, owing to the biphasic behaviour, it is possible that the $K_d$ of each binding site was not well determined. Interestingly, when similar ITC experiments were carried out for the interfacial single-mutant

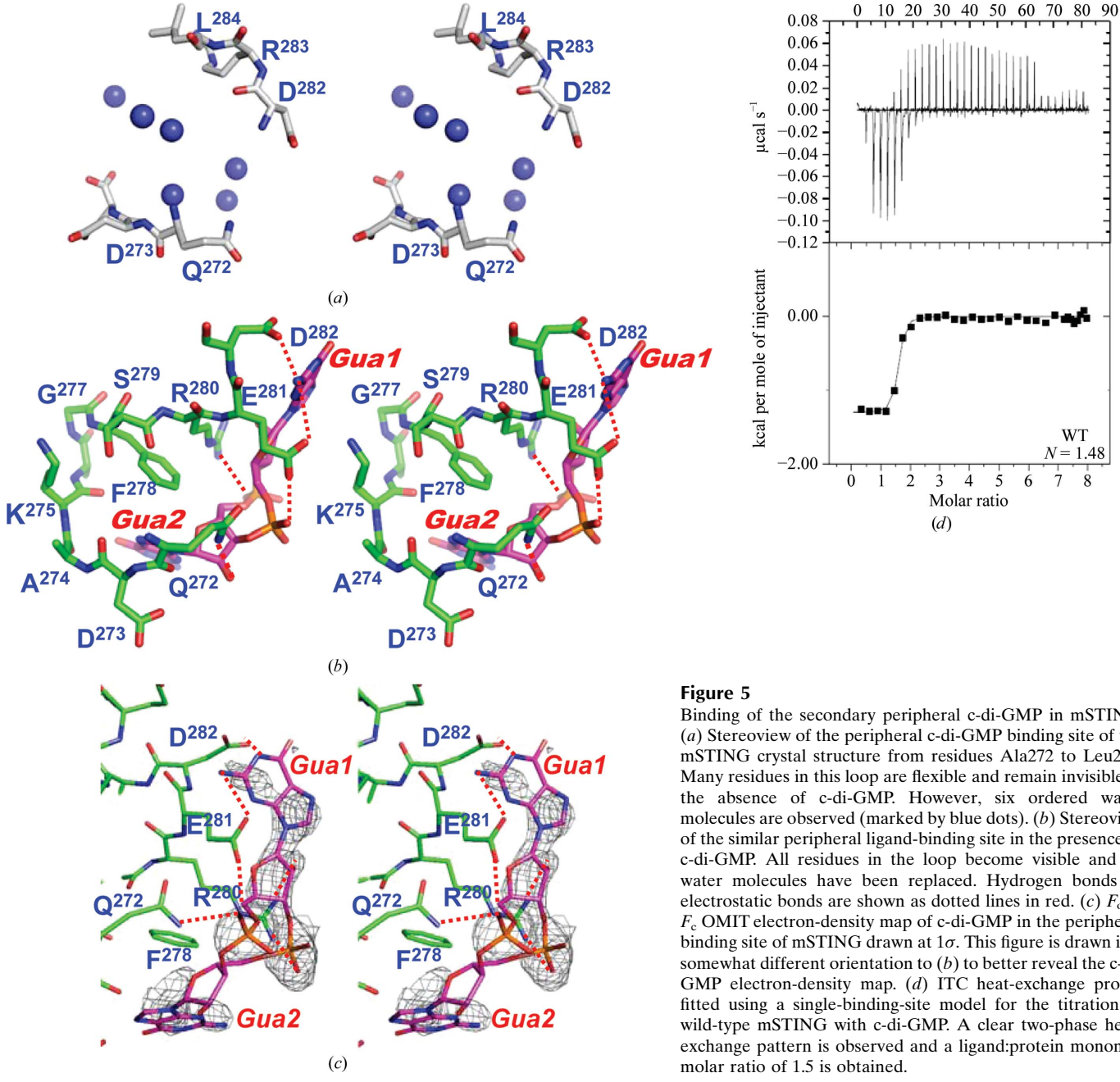


**Figure 5**
Binding of the secondary peripheral c-di-GMP in mSTING. (*a*) Stereoview of the peripheral c-di-GMP binding site of the mSTING crystal structure from residues Ala272 to Leu284. Many residues in this loop are flexible and remain invisible in the absence of c-di-GMP. However, six ordered water molecules are observed (marked by blue dots). (*b*) Stereoview of the similar peripheral ligand-binding site in the presence of c-di-GMP. All residues in the loop become visible and all water molecules have been replaced. Hydrogen bonds or electrostatic bonds are shown as dotted lines in red. (*c*) $F_o - F_c$ OMIT electron-density map of c-di-GMP in the peripheral binding site of mSTING drawn at 1$\sigma$. This figure is drawn in a somewhat different orientation to (*b*) to better reveal the c-di-GMP electron-density map. (*d*) ITC heat-exchange profile fitted using a single-binding-site model for the titration of wild-type mSTING with c-di-GMP. A clear two-phase heat-exchange pattern is observed and a ligand:protein monomer molar ratio of 1.5 is obtained.

variants, simple monophasic endothermic or exothermic titration curves were obtained (Fig. 5*e*), which could again be well fitted with a single-site model to obtain a $K_d$ ranging from $10^{-6}$ to $10^{-7}$ and a ligand:protein monomer molar ratio of 1 (Table 2). These results indicate that the disruption of crucial interfacial active-site residues (Ser161, Thr262 and Asn241; Fig. 4*d* and Table 2) enables mSTING to bind to c-di-GMP *via* the two equivalent peripheral binding sites with moderately strong binding affinity ($K_d$ of $10^{-6}$–$10^{-7}$). However, it is interesting to note that the titration profile of the T262A variant is endothermic, while those of the S161A and N241A variants are exothermic. Similarly, when ITC titration experiments were carried out for the two peripheral binding-site single-mutant variants, similar simple exothermic profiles were obtained that could also be well fitted using a single-site model to obtain a ligand:protein monomer molar ratio of 0.5 (Fig. 5*f*) with stronger binding affinities ($K_d$ ranging from $10^{-7}$ to $10^{-8}$; Table 2). These results indicated that disruption of the

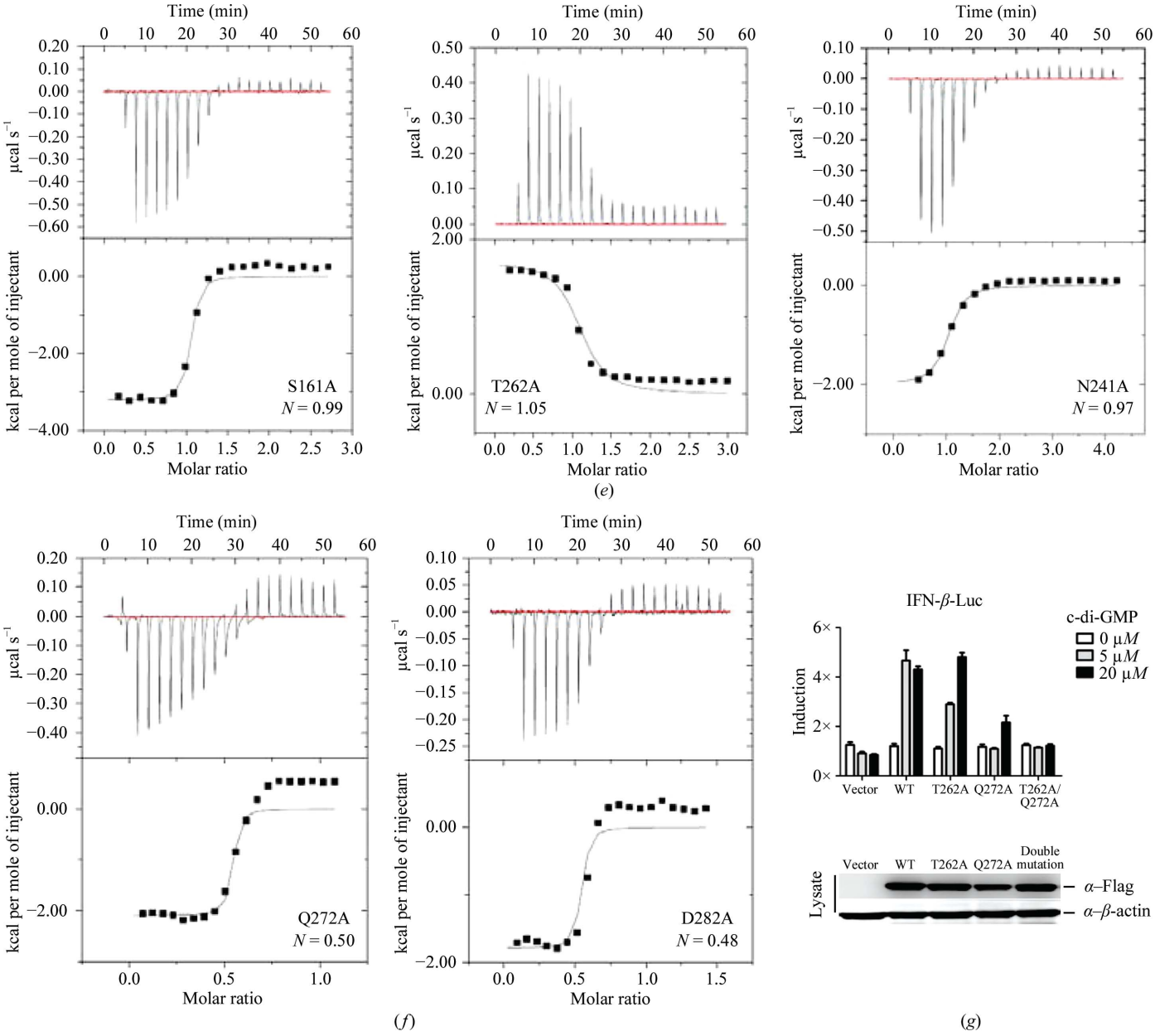


**Figure 5 (continued)**
(*e*) ITC exchange profiles for the mSTING single-mutant variants of the interfacial binding-site residues. A ligand:protein monomer molar ratio of approximately 1.0 is observed for the S161A, T262A and N241A variants. The T262A variant exhibits an endothermic profile different from the exothermic profiles observed for the S161A and N241A variants. (*f*) Similar ITC exchange profiles for the mSTING single-mutant variants of the peripheral binding-site residues. A ligand:protein monomer molar ratio of approximately 0.5 is observed for both the Q272A and D282A variants. (*g*) IFN-$\beta$ promoter luciferase reporter assay. HEK293T cells were cotransfected with Flag-fused full-length wild-type or mutated mSTING plasmids containing residues crucial for interfacial and peripheral c-di-GMP binding along with the IFN-$\beta$ and *Renilla* luciferase reporter plasmids. Luciferase activities were measured 16 h after stimulation with two different c-di-GMP concentrations as indicated. Values represent means of induction from three independent measurements, with the standard error marked by a vertical bar. Similar amounts of wild-type, T262A, Q272A and T262A/Q272A mSTING proteins are present in each cell lysate as detected by anti-Flag antibody.

crucial peripheral active-site residues (Gln272 and Asp282; Fig. 5*b* and Table 2) enables mSTING to bind c-di-GMP *via* the only interfacial binding site, although some residual heat absorption was observed at higher ligand:protein molar ratios, possibly owing to partial binding of c-di-GMP at the two peripheral sites. The extensive ITC studies of the wild-type and single-mutant mSTING variant proteins indicate that mSTING does contain three binding sites: one in the interfacial region and two in the peripheral region that are equivalent.

Binding of c-di-GMP to the three ligand-binding sites in wild-type mSTING may be allosterically controlled in either a positive or a negative way, and the $K_a$ of the c-di-GMP binding cannot be accurately determined when proteins exhibit such cooperative behaviour. However, the $K_a$ for wild-type mSTING has been determined to be approximately $5.4 \times 10^6\ M^{-1}$, which is somewhat stronger than the value determined for mSTING, using an *in vitro* UV-radiation cross-linking and dialysis-equilibrium assay method (Burdette *et al.*, 2011). Also, the ligand:protein monomer molar ratio determined from the ITC experiment ($N = 1.5$) is inconsistent with that determined by the dialysis method (Burdette *et al.*, 2011). The reason for this inconsistency is unclear. However, the dialysis method was carried out by irradiating an mSTING sample with radioactive c-di-GMP. The excess radioactive c-di-GMP was dialyzed away and the cross-linked radioactive mSTING–c-di-GMP adduct was checked for retained radioactivity. Obviously, when the cross-linking efficiency by UV irradiation of the complex does not reach 100%, nonconvalently bound c-di-GMP may be dialyzed away, rendering the obtained ligand:protein molar ratio and the measured $K_a$ value lower than expected. Since UV cross-linking efficiency is known to be low, a control may be required if such a method were used for ligand–protein or protein–protein binding-constant determination.

In order to further check whether the *in vitro* results using the N-terminally truncated mSTING protein are applicable *in vivo*, we also carried out an IFN-$\beta$ promoter luciferase assay by transfecting corresponding wild-type full-length mSTING or its variants into HEK293T cells to measure their luciferase activity. As shown in Fig. 5(*g*), when HEK293T cells were transfected with a wild-type mSTING plasmid and stimulated for 16 h in the presence of 5 or 20 µ*M* c-di-GMP, the luciferase activity increases more than fourfold, which is similar to that reported by Burdette *et al.* (2011). However, when Thr262, which is a crucial residue in binding interfacial c-di-GMP (Figs. 4*d* and 4*e*), is changed to Ala (the T262A variant), the luciferase activity decreased by approximately 50% when HEK293T cells were stimulated by 5 µ*M* c-di-GMP. However, no reduction was observed when HEK293T cells were stimulated by 20 µ*M* c-di-GMP. Interestingly, this diminishing effect is more pronounced in the Q272A mSTING variant, in which the altered amino acid Gln272 is involved in the peripheral c-di-GMP binding. The luciferase activity of the Q272A variant almost disappeared when HEK293T cells were stimulated by 5 µ*M* c-di-GMP and only approximately half of the activity remained when HEK293T cells were stimulated by 20 µ*M* c-di-GMP. Unsurprisingly, the luciferase activity of the mSTING T262A/Q272A double mutant almost disappeared when HEK293T cells were stimulated by either 5 or 20 µ*M* c-di-GMP. From these results, it seems to be that the peripheral c-di-GMP binding is more effective in promoting IFN-$\beta$ promoter activity than the interfacial c-di-GMP binding, and the alteration of a peripheral c-di-GMP binding residue (Gln272) can reduce the interfacial c-di-GMP binding of Thr262, leading to a more dramatic loss of luciferase activity. This may be a consequence of the fact that the peripheral ligand-binding site is more accessible to c-di-GMP than the interfacial binding site, since the peripheral ligand binding does not require the formation of the mSTING dimer.

## 4. Discussion

### 4.1. Structural comparison of ligand-binding specificity between mSTING–c-di-GMP and published hSTING–c-di-GMP complexes

After completion of this manuscript, four papers describing the crystal structures of the apo and c-di-GMP-bound forms of hSTING were reported (Huang *et al.*, 2012; Shang *et al.*, 2012; Shu *et al.*, 2012; Yin *et al.*, 2012). It is therefore interesting to compare these structures. However, a detailed comparison among them is beyond the scope of this study. We will therefore only describe the major distinct features that are correlated with the conclusions drawn from the present study. Basically, all of the reported apo-form hSTING crystal structures are more open than that of mSTING, with differing degrees of cross-subunit $\beta2$–$\beta3$ loop interactions. As expected, a stronger $\beta2$–$\beta3$ loop interaction seems to lead to a less open conformation of the STING dimers. For example, the apo form of hSTING published by Su's group (PDB entry 4f5e) has an intact $\beta2$–$\beta3$ loop structure (Huang *et al.*, 2012) and adopts a more closed form, while that of hSTING published by Wu's group (PDB entry 4f9e) has a barely observable $\beta2$–$\beta3$ loop interaction (Yin *et al.*, 2012) and adopts a more open form. For the c-di-GMP-bound hSTING complexes, there are similarities but also differences among the structures. In essence, the c-di-GMP molecules in these cocrystal structures all adopt a symmetrical guanine-base-exposed and upwards conformation with decent Tyr167 aromatic base/guanine base hydrophobic interactions which are similar to those in the cocrystal structure published by Liu's group (Ouyang *et al.*, 2012). Apart from these, there are substantial differences in the interactions of c-di-GMP with hSTING, especially in the inner ligand-binding cavity region. In the structure of Su and coworkers (PDB entry 4f5d), only weak interactions were observed between the Thr263 side chain and the c-di-GMP O2′ atom (Huang *et al.*, 2012). Two water molecules in the inner ligand-bound cavity are found to interact with the c-di-GMP lactone phosphate O atoms. However, good interactions of c-di-GMP with $\beta2$–$\beta3$ loop residues are observed, including those between the Ser241 carbonyl group and the guanine base $^1$N and $^2$N atoms and between the Arg238 side chain and the c-di-GMP lactone phosphate. In this paper, no other water molecule is reported. Strictly speaking, the specificity of c-di-

**Table 2**
Thermodynamic parameters for the binding of c-di-GMP to mSTING and its variants under the buffer condition 20 m*M* Tris–HCl pH 8.0, 80 m*M* NaCl measured by ITC.

All data were fitted using a single-binding-site model. NA, not available.

| Protein | $N$ | $K_a/K_d$ | $\Delta G$ (kcal mol$^{-1}$) | $\Delta H$ (kcal mol$^{-1}$) | $\Delta S$ (cal mol$^{-1}$ K$^{-1}$) |
|---|---|---|---|---|---|
| Wild type | 1.48 | $5.39 \times 10^6$/ $1.86 \times 10^{-7}$ | −9.1 | −1.3 ± 0.1 | 26.4 |
| Primary binding-site variants | | | | | |
| S161A | 0.99 | $5.95 \times 10^6$/ $1.68 \times 10^{-7}$ | −9.3 | −3.2 ± 0.1 | 20.3 |
| N241A | 0.97 | $4.53 \times 10^5$/ $2.21 \times 10^{-6}$ | −7.7 | −2.0 ± 0.1 | 19.2 |
| T262A | 1.05 | $3.79 \times 10^5$/ $2.64 \times 10^{-6}$ | −7.6 | +1.7 ± 0.1 | 31.3 |
| Y166A† | NA | NA | | | |
| R237A† | NA | NA | | | |
| E259A† | NA | NA | | | |
| Q265A† | NA | NA | | | |
| Secondary binding-site variants | | | | | |
| Q272A | 0.50 | $2.18 \times 10^7$/ $4.59 \times 10^{-8}$ | −9.9 | −8.3 ± 0.6 | 5.5 |
| D282A | 0.48 | $7.10 \times 10^6$/ $1.41 \times 10^{-7}$ | −9.3 | −1.7 ± 0.1 | 25.6 |
| F278A‡ | NA | NA | | | |
| R280A‡ | NA | NA | | | |
| E281A‡ | NA | NA | | | |
| Other variants | | | | | |
| G175L‡ | NA | NA | | | |
| I199N† | NA | NA | | | |
| Y313A† | NA | NA | | | |

† These variants formed inclusion bodies. ‡ These variants were unstable for ITC measurements.

GMP binding in this cocrystal structure is still weak and is mainly contributed by hydrogen bonds between the outer-cavity Ser241 backbone atoms and the c-di-GMP guanine base $^1$N and $^2$N atoms. In the structure of Xu and coworkers (PDB entry 4f5y), six water molecules situated in the inner cavity and five water molecules in the outer cavity are found to interact with c-di-GMP (Shang *et al.*, 2012). The binding specificity is mainly contributed by hydrogen bonds between the Thr263 side-chain O atom and the $^3$N and O2′ atoms of the c-di-GMP guanine base in the inner cavity region. There are also some water-mediated interactions with c-di-GMP from the $\beta2$–$\beta3$ loop residues such as Val239 and Arg238 in the outer cavity region. The specificity of c-di-GMP binding in this cocrystal structure is somewhat stronger, but still contains a large number of water-mediated interactions. Similarly, in the structure of Li and coworkers (PDB entry 4emt), specific interactions between the Thr263 side chain and the $^3$N and O2′ atoms of the c-di-GMP guanine base in the inner cavity region were also discovered (Shu *et al.*, 2012). However, quite a few inner cavity water molecules (approximately ten) and more than ten outer cavity water molecules are found. Since the $\beta2$–$\beta3$ loop residues are mostly invisible near the c-di-GMP binding region in this cocrystal structure, no specific interaction in the outer cavity region was found. This case is more similar to the initially published mSTING cocrystal structure (PDB entry 4ef4) by Liu's group (Ouyang *et al.*, 2012). Finally, in the structure of Wu and coworkers (PDB entry 4f9g) the ligand–protein interaction is quite weak (Yin *et al.*, 2012): no water molecule is reported in the deposited coordinate file and only two hydrogen bonds between the Thr263 side-chain atom and the O2′ and $^3$N atoms of c-di-GMP are observed in the inner cavity region. No strong interactions from the outer cavity, either direct or indirect, are observed either, possibly owing to the highly disordered nature of the $\beta2$–$\beta3$ loop residues near the ligand-binding site. In conclusion, all of the reported hSTING cocrystal structures have few direct protein–ligand interactions in the inner cavity region and most of the interactions between hSTING and c-di-GMP are contributed from water-mediated binding.

### 4.2. The closed-form mSTING–c-di-GMP complex possibly arises from c-di-GMP binding to an open form similar to that of apo hSTING followed by a further c-di-GMP tumbling and induced-fit process

Unlike hSTING, the apo and c-di-GMP-bound forms of mSTING all adopt closed-form conformations. Obviously, a ligand cannot obtain access to the active site of the closed unliganded form to attain a closed liganded complex. We suggest that the closed and open unliganded forms of STING are in equilibrium and that free c-di-GMP adopting different conformations can interact with the open unliganded form. During this initial encounter, only a suitable c-di-GMP conformer is selected to form a recognition complex and the $\pi$-helix element in the mSTING structure may be important in forming such a recognition complex (Fig. 3*b* and Supplementary Fig. S3). At this stage, the mSTING protein is still in the open form and possibly adopts a conformation similar to that reported for the hSTING–c-di-GMP complex. After further c-di-GMP reorganization (tumbling and flipping), which is possibly accelerated by the binding of c-di-GMP at the peripheral sites, the interfacial c-di-GMP can rearrange to form a more compact and stable mSTING–c-di-GMP complex (Fig. 4*d*) through a large-scale induced-fit process. In fact, the bound c-di-GMP in the mSTING complex adopts the most compact conformation observed to date, containing two intramolecular interactions (Gua2 N2 to Gua2 phosphate and Gua2 N2 to Gua1 O4′; Fig. 4*d*), and exhibits considerable hydrophobic interaction with the wedged Thr262 residue (Figs. 4*d* and 4*e*).

Such a STING–c-di-GMP interaction scenario seems to be reasonable based on entropy considerations. c-di-GMP is a highly polar doubly charged species that contains a hydration shell in solution. This hydrated c-di-GMP seems to interact with the binding site in the recognition complex without much conformational change, as reflected by the fact that the ligand-binding site of the reported hSTING–c-di-GMP complex structure still contains many water molecules, and c-di-GMP was found to mainly interact indirectly with hSTING through water molecules, as described above. This indicates that little entropic gain could be obtained after forming such a recognition complex. Reorganization of c-di-GMP is thus crucial for the complex to reach the final state, which is accomplished *via* further c-di-GMP tumbling and flipping to interact specifically with many active-site residues of mSTING (Fig. 4*d*) without

water intervention. This reorganization process can gain much entropy by releasing many water molecules from the original mSTING central cavity (Fig. 4*c*) and the hydration shell of c-di-GMP.

Although two different c-di-GMP ligand conformations were observed, it is unclear at present whether the more open form of the hSTING–c-di-GMP complex or the more closed-form mSTING–c-di-GMP complex is more physiologically relevant. Furthermore, it is also unclear whether c-di-GMP binding at the peripheral sites plays a role in interaction with the transmembrane domain or in interaction with TBK1 or IRF to enhance IFN-$\beta$ production. Further studies are necessary to clarify these issues.

### 4.3. Why do hSTING and mSTING adopt different apo and c-di-GMP-bound crystal structures?

To date, five structures of hSTING in apo and c-di-GMP-bound forms have been reported (Huang *et al.*, 2012; Ouyang *et al.*, 2012; Shu *et al.*, 2012; Su *et al.*, 2012; Yin *et al.*, 2012). Interesting, they all seem to adopt a similar set of open-form structures, which are different to the closed-form structures of mSTING that we have described in this manuscript. Therefore, it would be interesting to know why these two STING proteins adopt very different crystal structures even though they have considerable sequence identity (69%). One reason may be that the two sequences are not the same and are still approximately 30% different. Another reason may result from the different crystallization conditions. To explore this issue, we have listed the screening conditions for the formation of the STING–c-di-GMP complex crystals published to date in Supplementary Table S6. We found that the parameter most potentially characteristic of unique mSTING complex crystal formation is the ligand:protein molar ratio used: while most hSTING proteins were cocrystallized with c-di-GMP using a ligand:protein molar ratio of 1.0 or 0.5, our mSTING protein was cocrystallized with c-di-GMP at a molar ratio of 2.0 according to the ITC data that we obtained. Since a molar ratio of at least 1.5 is necessary for c-di-GMP to fully occupy the potential ligand-binding sites of mSTING, we suspect that an insufficient amount of c-di-GMP only allows hSTING to accommodate one c-di-GMP to form the reported hSTING–c-di-GMP complex structure. We are currently investigating this issue by cocrystallizing STING proteins at different c-di-GMP:protein molar ratios.

### 4.4. The closed form of the mSTING–c-di-GMP complex is consistent with previous and current biophysical data

Our newly determined closed-form complex structure, although unique, is also compatible with most of the available biophysical and biochemical data reported for the mSTING–c-di-GMP complex. For example, it was found that an I199N mSTING mutant in Goldenticket mice abolishes its function to stimulate IFN-$\beta$ production (Burdette *et al.*, 2011). From our determined structure, we find that residue Ile199 plays a crucial role in forming the hydrophobic core of mSTING. It is extensively surrounded by hydrophobic residues such as Leu197, Cys308, Leu310, Phe201, Ala261, Tyr162 and the side-chain atoms of Glu259 (Supplementary Fig. S2*c*). In addition, the I199N variant was indeed found to cause mSTING to form an inclusion body without correct folding (data not shown). Similarly, another variant, mut22 (Y313A), is also important in stabilizing a hydrophobic cluster that includes residues Ile311, Leu200, Pro202, Phe322, Leu324 and the side-chain atoms of Glu315 and Glu327 (not shown). The Y313A variant also caused mSTING to form an inclusion body in a similar way. These two residues are nearby and the hydrophobic cores they form collectively set up the boundary for accommodating c-di-GMP at the two sides (Supplementary Fig. S2*c*). Some of the residues forming these hydrophobic clusters are boxed in grey in Fig. 1(*a*). Residues Glu259 and Gln265 in the mut11 class are directly involved in binding c-di-GMP (Fig. 4*d*). The side chain of Gln265 forms two hydrogen bonds to the Gua1 N1 and O6 atoms, and the side chain of Glu259 forms a good hydrogen bond to the side-chain O atom of Tyr166, which stacks very well with the Gua2 base. Residues Asp209, Asp215 and Asn217 in the mut8 class are not directly involved in c-di-GMP binding according to our determined structure. However, these residues have a strong tendency to locate in a loop–turn region (Williams *et al.*, 1987) and their presence in the $P^{208}$DN or $D^{215}$PN loop–turns (Fig. 1*a*) may be important for mSTING to form the correct tertiary structure. Regarding residues Tyr239, Ser242 and Tyr244 in the mut10 class, the side chain of Tyr239 also forms a direct hydrogen bond to the phosphate of c-di-GMP (Fig. 4*d*). Tyr244 also forms a strong hydrophobic cluster nearby that includes residues Phe220, Val213, Ile218 and Phe240 (not shown). For the mutations in the residue bundle mut13, which includes residues Arg280, Glu281, Asp282, Arg283, Glu285, Gln286 and Lys288 located in the $\alpha$7–$\alpha$8 loop, the reason is obvious as residues Arg280, Glu281 and Asp282 are found to participate in forming the peripheral c-di-GMP binding site (Figs. 1*a* and 5*b*). Finally, residues Ser162, Tyr167 and Thr263 in hSTING have been found to be essential in binding c-di-GMP (Ouyang *et al.*, 2012). These are also the residues involved in direct binding to c-di-GMP (Ser161, Tyr166 and Thr262 in mSTING; Fig. 4*d*).

### 4.5. Interfacial c-di-GMP in the mSTING complex adopts the most compact conformation reported to date

How c-di-GMP can bind to so many different effectors and perform so many diverse functions is an interesting issue worthy of intensive investigation (Sondermann *et al.*, 2011; Krasteva *et al.*, 2012; Ryan *et al.*, 2012). Recently, it has been proposed that the structural polymorphism of c-di-GMP adds another level of complexity to its function (Römling, 2012). Indeed, in addition to the regular closed-form c-di-GMP (Fig. 6*a*) binding to the type I PilZ domain or the open-form c-di-GMP binding to the EAL domain (Fig. 6*b*), we have discovered several unique conformations of c-di-GMP in its monomeric or dimeric state. For example, we have found that a c-di-GMP dimer can bind at the GGDEF dimeric interface and adopt a novel dimeric conformation to bind in the active site of a HAMP-GGDEF protein to inhibit its diguanylate

activity *via* a product feedback-inhibition mode (Yang *et al.*, 2011). Also, c-di-GMP can adopt a bulged form when it interacts with the degenerate *Xcc*FimX$^{EAL}$ domain (Fig. 6*d*) or can adopt an open twisted form when it interacts with the *Xcc*FimX$^{EAL}$–type II PilZ complex (Fig. 6*c*; Chin *et al.*, 2012). We show these different c-di-GMP conformers in Fig. 6, with the Gua1 of each conformer superimposed and circled by a dotted red line. From this presentation, one can see that different c-di-GMP conformers can be achieved by altering the 12-membered ring torsional angles ($\alpha$, $\beta$, $\gamma$, $\delta$, $\varepsilon$ or $\zeta$; Fig. 6*b*), by a C3′-*endo* to C2′-*endo* transformation (Fig. 6*c*) or by altering the glycosidic torsional angle ($\chi$; Fig. 6*d*). It is interesting to note that the $\chi$ angles of the c-di-GMP Gua2 base in both the FimX$^{EAL}$ (Fig. 6*d*) and the mSTING complexes (Fig. 6*e*) are in an unusual *syn* configuration. Thus, c-di-GMP seems to be quite flexible and can change its conformation without a large energy barrier to fit to a plethora of different recognition motifs. When interacting with mSTING as reported in the present manuscript, c-di-GMP even adopts a novel compact form that has not previously been observed to date. This compact form exhibits considerable hydrophobic interaction between the two guanine bases and forms two hydrogen bonds between the Gua2 base and the Gua1 ribose and phosphate O atoms (Figs. 4*d*, 4*e* and 6*e*). Such a compact conformation may be able to help to close the valley between the two mSTING monomers to form a more closed-form conformation (Fig. 2*b*).

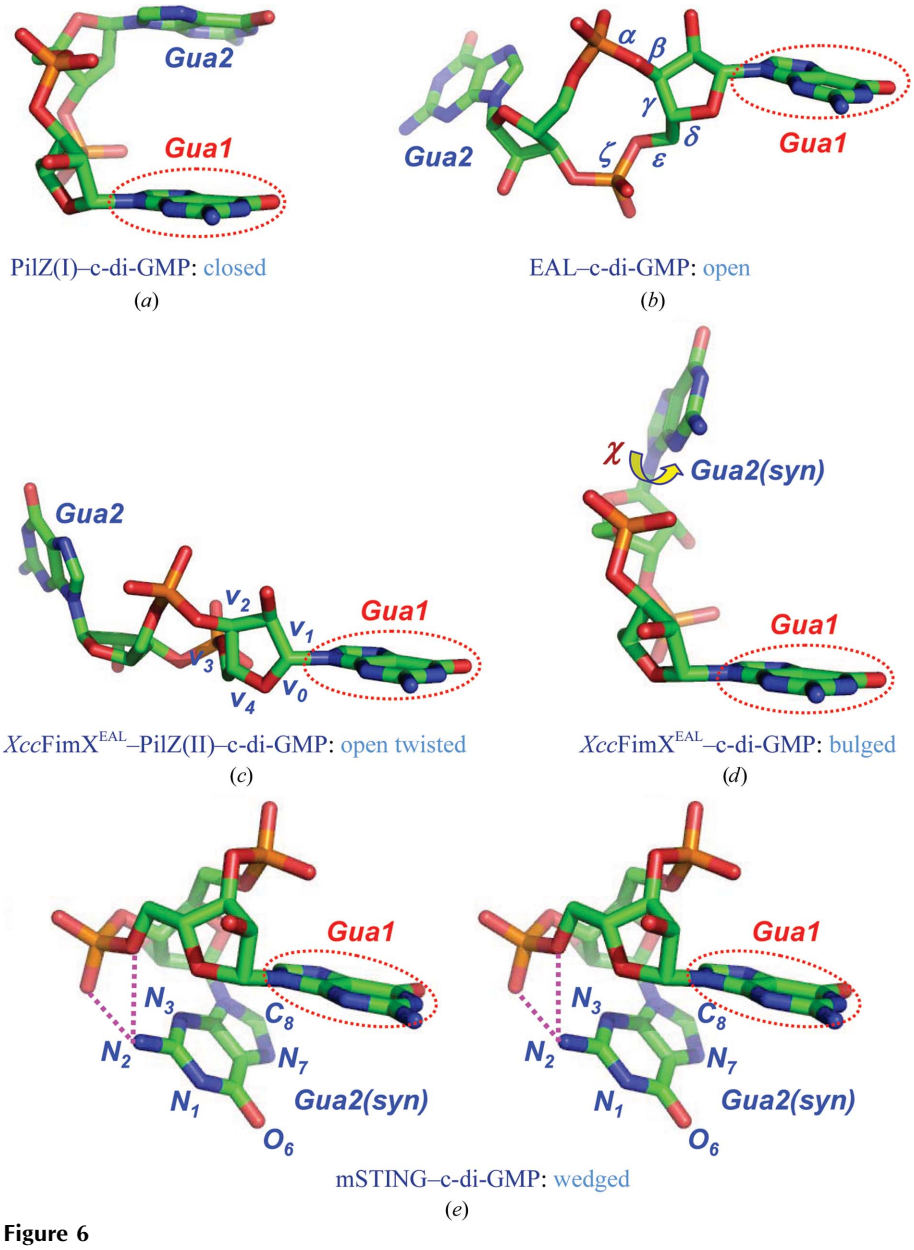


**Figure 6**
Overview of the monomeric c-di-GMP conformers reported to date. They are superimposed based on the Gua1 base (circled by a dotted red line) and plotted individually. N atoms are coloured blue, O atoms red, P atoms orange and C atoms green. The coordinates for (*a*), (*b*), (*c*) and (*d*) are from PDB entries 2rde, 3hv8, 4f48 and 4f3h, respectively. The typical 12-membered torsional angles are shown in (*b*), the sugar torsional angles are shown in (*c*) and the naming system for the guanine base is shown in (*e*) as a stereoview. Gua2 in (*d*) and (*e*) adopts an unusual *syn*-glycosidic angle (marked $\chi$ in *d*).

## 5. Conclusion

We have solved the structures of the apo and c-di-GMP-bound forms of the C-terminal domain of mouse STING, which yield new insights into how the receptor proteins bind and recognize bacterial messenger c-di-GMP. Firstly, the mSTING structure adopts a more closed-form conformation compared with the more open form reported for hSTING proteins. Secondly, c-di-GMP binds in the primary binding site at the dimeric interface through extensive and direct interactions with mSTING amino-acid side chains, in contrast to the largely water-mediated network interaction in hSTING proteins. Thirdly, two unexpected secondary c-di-GMP-binding sites were identified in the structure and were validated using crystal and solution studies. All observations seem to indicate that the present mSTING–c-di-GMP structure may represent a stable binding complex that could be physiologically relevant. It may facilitate the rational design of immunostimulatory drugs that target the intracellular nucleic acid-sensing pathways.

This work was supported in part by the Ministry of Education, Taiwan, ROC under the ATU plan and by the National Science Council, Taiwan, ROC (grant 97-2113-M005-005-MY3 to S-HC). We appreciate the Structural Genomics Databases service provided

by the GMBD Bioinformatics Core (http://www.tbi.org.tw), NRPGM, Taiwan, ROC. We would also like to thank the Core Facilities for Protein X-ray Crystallography in the Academia Sinica, Taiwan, ROC for help in crystal screening, and the National Synchrotron Radiation Research Center (NSRRC) in Taiwan and the SPring-8 synchrotron facility in Japan for assistance in X-ray data collection. The National Synchrotron Radiation Research Center is a user facility supported by the National Science Council, Taiwan, ROC; the Protein Crystallography Facility is supported by the National Research Program for Genomic Medicine, Taiwan, ROC.

## References

Adams, P. D. *et al.* (2010). *Acta Cryst.* D**66**, 213–221.
Amikam, D. & Galperin, M. Y. (2006). *Bioinformatics*, **22**, 3–6.
Aparicio, R., Ferreira, S. T. & Polikarpov, I. (2003). *J. Mol. Biol.* **334**, 1023–1041.
Barbalat, R., Ewald, S. E., Mouchess, M. L. & Barton, G. M. (2011). *Annu. Rev. Immunol.* **29**, 185–214.
Barber, G. N. (2011). *Curr. Opin. Immunol.* **23**, 10–20.
Benach, J., Swaminathan, S. S., Tamayo, R., Handelman, S. K., Folta-Stogniew, E., Ramos, J. E., Forouhar, F., Neely, H., Seetharaman, J., Camilli, A. & Hunt, J. F. (2007). *EMBO J.* **26**, 5153–5166.
Bermejo, G. A., Strub, M. P., Ho, C. & Tjandra, N. (2010). *Biochemistry*, **49**, 1893–1902.
Brünger, A. T., Adams, P. D., Clore, G. M., DeLano, W. L., Gros, P., Grosse-Kunstleve, R. W., Jiang, J.-S., Kuszewski, J., Nilges, M., Pannu, N. S., Read, R. J., Rice, L. M., Simonson, T. & Warren, G. L. (1998). *Acta Cryst.* D**54**, 905–921.
Burdette, D. L., Monroe, K. M., Sotelo-Troha, K., Iwig, J. S., Eckert, B., Hyodo, M., Hayakawa, Y. & Vance, R. E. (2011). *Nature (London)*, **478**, 515–518.
Chen, V. B., Arendall, W. B., Headd, J. J., Keedy, D. A., Immormino, R. M., Kapral, G. J., Murray, L. W., Richardson, J. S. & Richardson, D. C. (2010). *Acta Cryst.* D**66**, 12–21.
Chin, K.-H., Kuo, W.-T., Yu, Y.-J., Liao, Y.-T., Yang, M.-T. & Chou, S.-H. (2012). *Acta Cryst.* D**68**, 1380–1392.
Chin, K.-H., Lee, Y.-C., Tu, Z.-L., Chen, C.-H., Tseng, Y.-H., Yang, J.-M., Ryan, R. P., McCarthy, Y., Dow, J. M., Wang, A. H.-J. & Chou, S.-H. (2010). *J. Mol. Biol.* **396**, 646–662.
Cooley, R. B., Arp, D. J. & Karplus, P. A. (2010). *J. Mol. Biol.* **404**, 232–246.
Floceo, M. M. & Mowbray, S. L. (1994). *J. Biol. Chem.* **269**, 8930–8936.
Hengge, R. (2009). *Nature Rev. Microbiol.* **7**, 263–273.
Hornung, V. & Latz, E. (2010). *Nature Rev. Immunol.* **10**, 123–130.
Huang, Y.-H., Liu, X.-Y., Du, X.-X., Jiang, Z.-F. & Su, X.-D. (2012). *Nature Struct. Mol. Biol.* **19**, 728–730.
Ishikawa, H. & Barber, G. N. (2008). *Nature (London)*, **455**, 674–678.
Jin, L., Hill, K. K., Filak, H., Mogan, J., Knowles, H., Zhang, B., Perraud, A.-L., Cambier, J. C. & Lenz, L. L. (2011). *J. Immunol.* **187**, 2595–2601.
Karaolis, D. K., Means, T. K., Yang, D., Takahashi, M., Yoshimura, T., Muraille, E., Philpott, D., Schroeder, J. T., Hyodo, M., Hayakawa, Y., Talbot, B. G., Brouillette, E. & Malouin, F. (2007). *J. Immunol.* **178**, 2171–2181.
Kawai, T. & Akira, S. (2010). *Nature Immunol.* **11**, 373–384.
Krasteva, P. V., Giglio, K. M. & Sondermann, H. (2012). *Protein Sci.* **21**, 929–948.
Krissinel, E. & Henrick, K. (2007). *J. Mol. Biol.* **372**, 774–797.
Kulshina, N., Baird, N. J. & Ferré-D'Amaré, A. R. (2009). *Nature Struct. Mol. Biol.* **16**, 1212–1217.
Leduc, J. L. & Roberts, G. P. (2009). *J. Bacteriol.* **191**, 7121–7122.
Lin, S.-H. & Lee, J. C. (2002). *Biochemistry*, **41**, 11857–11867.
McRee, D. E. (1999). *J. Struct. Biol.* **125**, 156–165.
McWhirter, S. M., Barbalat, R., Monroe, K. M., Fontana, M. F., Hyodo, M., Joncker, N. T., Ishii, K. J., Akira, S., Colonna, M., Chen, Z. J., Fitzgerald, K. A., Hayakawa, Y. & Vance, R. E. (2009). *J. Exp. Med.* **206**, 1899–1911.
Navarro, M. V., De, N., Bae, N., Wang, Q. & Sondermann, H. (2009). *Structure*, **17**, 1104–1116.
Ouyang, S., Song, X., Wang, Y., Ru, H., Shaw, N., Jiang, Y., Niu, F., Zhu, Y., Qiu, W., Parvatiyar, K., Li, Y., Zhang, R., Cheng, G. & Liu, Z.-J. (2012). *Immunity*, **36**, 1073–1086.
Passner, J. M. & Steitz, T. A. (1997). *Proc. Natl Acad. Sci. USA*, **94**, 2843–2847.
Rao, F., Pasunooti, S., Ng, Y., Zhuo, W., Lim, L., Liu, A. W. & Liang, Z.-X. (2009). *Anal. Biochem.* **389**, 138–142.
Rathinam, V. A. & Fitzgerald, K. A. (2011). *Curr. Opin. Virol.* **1**, 455–462.
Römling, U. (2012). *Environ. Microbiol.* **14**, 1817–1829.
Römling, U., Gomelsky, M. & Galperin, M. Y. (2005). *Mol. Microbiol.* **57**, 629–639.
Ryan, R. P., Tolker-Nielsen, T. & Dow, J. M. (2012). *Trends Microbiol.* **20**, 235–242.
Sauer, J. D., Sotelo-Troha, K., von Moltke, J., Monroe, K. M., Rae, C. S., Brubaker, S. W., Hyodo, M., Hayakawa, Y., Woodward, J. J., Portnoy, D. A. & Vance, R. E. (2011). *Infect. Immun.* **79**, 688–694.
Schirmer, T. & Jenal, U. (2009). *Nature Rev. Microbiol.* **7**, 724–735.
Shang, G., Zhu, D., Li, N., Zhang, J., Zhu, C., Lu, D., Liu, C., Yu, Q., Zhao, Y., Xu, S. & Gu, L. (2012). *Nature Struct. Mol. Biol.* **19**, 725–727.
Shu, C., Yi, G., Watts, T., Kao, C. C. & Li, P. (2012). *Nature Struct. Mol. Biol.* **19**, 722–724.
Smith, K. D., Lipchock, S. V., Ames, T. D., Wang, J., Breaker, R. R. & Strobel, S. A. (2009). *Nature Struct. Mol. Biol.* **16**, 1218–1223.
Sondermann, H., Shikuma, N. J. & Yildiz, F. H. (2011). *Curr. Opin. Microbiol.* **15**, 140–146.
Su, Y.-C., Tu, Z.-L., Yang, C.-Y., Chin, K.-H., Chuah, M. L.-C., Liang, Z.-X. & Chou, S.-H. (2012). *Acta Cryst.* F**68**, 906–910.
Sun, W., Li, Y., Chen, L., Chen, H., You, F., Zhou, X., Zhou, Y., Zhai, Z., Chen, D. & Jiang, Z. (2009). *Proc. Natl Acad. Sci. USA*, **106**, 8653–8658.
Takeuchi, O. & Akira, S. (2010). *Cell*, **140**, 805–820.
Tanaka, Y. & Chen, Z. J. (2012). *Sci. Signal.* **5**, ra20.
Tao, F., He, Y.-W., Wu, D.-H., Swarup, S. & Zhang, L.-H. (2010). *J. Bacteriol.* **192**, 1020–1029.
Terwilliger, T. C., Adams, P. D., Read, R. J., McCoy, A. J., Moriarty, N. W., Grosse-Kunstleve, R. W., Afonine, P. V., Zwart, P. H. & Hung, L.-W. (2009). *Acta Cryst.* D**65**, 582–601.
Terwilliger, T. C., Grosse-Kunstleve, R. W., Afonine, P. V., Moriarty, N. W., Zwart, P. H., Hung, L.-W., Read, R. J. & Adams, P. D. (2008). *Acta Cryst.* D**64**, 61–69.
Vandeyar, M. A., Weiner, M. P., Hutton, C. J. & Batt, C. A. (1988). *Gene*, **65**, 129–133.
Weaver, T. M. (2000). *Protein Sci.* **9**, 201–206.
Williams, R. W., Chang, A., Juretić, D. & Loughran, S. (1987). *Biochim. Biophys. Acta*, **916**, 200–204.
Woodward, J. J., Iavarone, A. T. & Portnoy, D. A. (2010). *Science*, **328**, 1703–1705.
Xiong, A.-S., Peng, R.-H., Zhuang, J., Gao, F., Li, Y., Cheng, Z.-M. & Yao, Q.-H. (2008). *FEMS Microbiol. Rev.* **32**, 522–540.
Yang, C.-Y., Chin, K.-H., Chuah, M. L.-C., Liang, Z.-X., Wang, A. H.-J. & Chou, S.-H. (2011). *Acta Cryst.* D**67**, 997–1008.
Yin, Q., Tian, Y., Kabaleeswaran, V., Jiang, X., Tu, D., Eck, M. J., Chen, Z. J. & Wu, H. (2012). *Mol. Cell*, **46**, 735–745.
Zhong, B., Yang, Y., Li, S., Wang, Y.-Y., Li, Y., Diao, F., Lei, C., He, X., Zhang, L., Tien, P. & Shu, H.-B. (2008). *Immunity*, **29**, 538–550.